Diagnostic sensitivity of SPECT myocardial perfusion imaging using a pumping cardiac phantom with inserted variable defects

Isabelle Chrysanthou-Baustert, PhD,[a] Yiannis Parpottas, PhD,[a,b] Ourania Demetriadou, MD,[c] Stelios Christofides, PhD,[d,e] Charalambos Yiannakkaras, MSc,[e] Demetris Kaolis, MSc[d,e] Marta Wasilewska-Radwanska, PhD,[f] Tomasz Fiutowski, PhD,[f] and Franciszek Sikora, BSc[f]

Background. **The diagnostic sensitivity of various SPECT MPI procedures was assessed using a pumping cardiac phantom with variable defects inserted in the myocardial wall of the left ventricle.**

Methods and Results. **A diagnostic evaluation of 142 myocardial defects was performed. A diagnosis blinded to prior-known conditions was compared to the known defects severity (transmural, subendocardial) and defects position within the myocardial wall of the left ventricle (apical, anterior, inferior) for three body types (average male, large male, large female). Non-attenuation corrected, attenuation corrected and gated SPECT MPI were performed. The diagnostic sensitivity was improved when applying attenuation correction or gating techniques to identify subendocardial defects in the inferior, anterior and apical segments of the myocardial wall of the left ventricle for all three body types. Transmural defects could be identified without any attenuation correction or gating.**

Conclusions. **The diagnostic sensitivity was improved when applying AC or GSPECT techniques. (J Nucl Cardiol 2013;20:609–15.)**

Key Words: Myocardial perfusion imaging (MPI) • gated SPECT (GSPECT) • attenuation correction (AC) • pumping cardiac phantom • variable defects

INTRODUCTION

Coronary artery disease (CAD) is the most common form of heart disease worldwide. Statistics show that CAD is one of the leading causes of death for both men and women in Europe and in the United States.[1,2] Once CAD is detected, the condition should be closely monitored and appropriate steps should be taken to prevent deterioration or death. Myocardial perfusion imaging (MPI) has been proven to be able to assess the functional significance of a coronary artery stenosis.[3]

In recent years, radionuclide-imaging technologies have evolved rapidly with the development of new instrumentation in an attempt to accurately perform attenuation correction with validated commercial hardware/software solutions that enhances the interpretive confidence and accuracy of single photon emission computed tomography (SPECT) myocardial perfusion studies.[4-6] Various studies highlight the benefits of attenuation correction and/or gating in MPI. Nevertheless, some studies failed to demonstrate improvement or increased specificity at the cost of sensitivity.[7,8] While analytic models and patient data are useful, a reproducible, compartmented, mechanical phantom is also useful to compare and optimize MPI studies without exposing patients to radiation.

This study investigated the diagnostic sensitivity of non-attenuation corrected (NC), attenuation corrected

From the Frederick Research Centre,[a] Nicosia, Cyprus; General Department (Physics-Mathematics),[b] Frederick University, Nicosia, Cyprus; Nuclear Medicine Department,[c] Limassol General Hospital, Limassol, Cyprus; Biomedical Research Foundation,[d] Nicosia, Cyprus; Medical Physics Department,[e] Nicosia General Hospital, Nicosia, Cyprus; and AGH University of Science and Technology,[f] Kraków, Poland.

This research was funded by the Cyprus Research Promotion Foundation and the European Regional Development Fund through the project ΥΓΕΙΑ/ΔΥΓΕΙΑ/0308/11 (BIE).

Received for publication Apr 11, 2012; final revision accepted Apr 29, 2013.

Reprint requests: Isabelle Chrysanthou-Baustert, PhD, Frederick Research Centre, Nicosia, Cyprus; *isabelle.chrysanthou@gmail.com*.

1071-3581/$34.00

doi:10.1007/s12350-013-9726-y

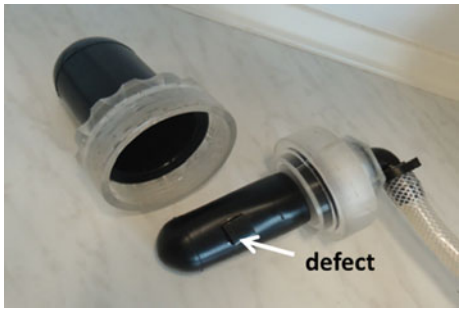

Figure 1. The small and large rubber membranes of the cardiac phantom. The small membrane is mounted inside the larger membrane, both kept in position by a holder. The inner membrane defines the left ventricular cavity, while the space between the inner and the outer membrane represents the myocardial wall of the left ventricle. A solid defect is glued on the outer part of the inner membrane.

(AC) and gated SPECT (GSPECT) techniques for transmural and subendocardial defects (a) in three body types and (b) in the three main areas of left ventricle. For this purpose, we utilized a custom-built pumping heart phantom with inserted defects, varying in severity and position, to experimentally simulate CAD.

MATERIALS AND METHODS

We performed 43 acquisitions using a custom-built pumping heart phantom resulting in a total of 142 evaluated myocardial defects. The phantom, acquisition and reconstruction parameters as well as the images and the physician's report were stored in a database to compare the prior-known parameters with the blinded diagnosis.

Dynamic Cardiac Phantom and Defects

The dynamic cardiac phantom consisted of (a) a twin-membrane system representing the left ventricle, (b) a pumping system and (c) a computer-controlled system. The cardiac phantom is based on a twin-membrane where a small rubber membrane is mounted inside a larger rubber membrane. Both membranes are kept in position by a holder, as shown in Figure 1. The inner membrane defines the left ventricular cavity, while the space between the inner and the outer membrane represents the myocardial wall of the left ventricle.

The ellipsoid membranes of 1 mm thickness expand during the diastole and retract during the systole into their initial shape without being stretched with time due to the material characteristics. The membranes were manufactured through the process of injection moulding. The thickness of the myocardial wall of the left ventricle at systole was 12 mm and at diastole was 11 mm.

Diastole and systole were achieved by pumping water in and out the inner membrane. For this purpose, a piston was activated by a stepper motor which was controlled by a computer. As the cavity between the inner and the outer membrane was filled with water which is non-compressive, the pressure was transferred from the inner to the outer membrane. For the imaging procedures, a diluted radionuclide was also injected within the myocardial wall. Figure 2 shows the twin-membrane system during expansion and compression.

Figure 2. The cardiac phantom during expansion (diastole) and compression (systole).

The studies have been performed at 60 beats per min. The ejection fraction was $30 \pm 3\%$. This was obtained from measurements of the end-systole-volume (ESV) and the end-diastole-volume (EDV) of the cardiac phantom, and it was also compared with the corresponding values obtained from the processing workstations. For the gated studies, the signal from an ECG simulator was used as an input to the ECG device whose exit signal triggered the SPECT and the computer-controlled pumping system.

One or multiple defects were placed at specific locations in the spacing between the inner and outer membranes to represent specific coronary obstruction, according to the segmentation model of the left ventricle.[9] Transmural (1 cm in thickness) and subendocardial (0.5 cm in thickness) defects, of 2×2 cm and 1.5×1.5 cm in extent, glued on the outer part of the inner membrane (Figure 1), were placed in the apical, the anterior and the inferior regions of the myocardial wall of the left ventricle. More cardiac phantoms were constructed to simulate different combinations of defects. When using a transmural solid defect (100% reduction in flow through the myocardial wall), it is expected to measure a 100% reduction in flow, while when using a subendocardial solid defect (100% reduction in flow in only half of the myocardial wall), it is expected to measure a 50% reduction in flow. In reality, defects may be due to an incomplete reduction in flow which is not modeled by this phantom. Simulations have shown that due to partial volume effects, a small defect with 100% reduction in flow and a larger defect with 50% flow reduction will appear the same with conventional technology.[10,11]

For the MPI, the cardiac phantom was inserted within the RSD Anderson fully tissue equivalent anthropomorphic phantom to simulate the scattering and the non-uniform attenuating environment introduced by the thoracic structures.[12] The thorax phantom represents an average male. With the addition of the thorax overlay, it could represent a large male. Adding the breasts on the thorax overlay, it could represent a large female. The thorax containing the lungs and the pumping heart was hermetically closed and then the rest of the thorax cavity was completely filled with water to simulate the soft tissue. Figure 3 shows the large female (left) and the average male (right) body types of the anthropomorphic phantom in the Philips Forte/Vantage SPECT/^{153}Gd.

Figure 4 shows transverse chest CT slices of a normal heart (left) and the cardiac phantom at diastole (right) inserted

Figure 3. The large female (*left*) and the average male (*right*) body types of the anthropomorphic phantom in the Philips Forte/Vantage SPECT/^{153}Gd.

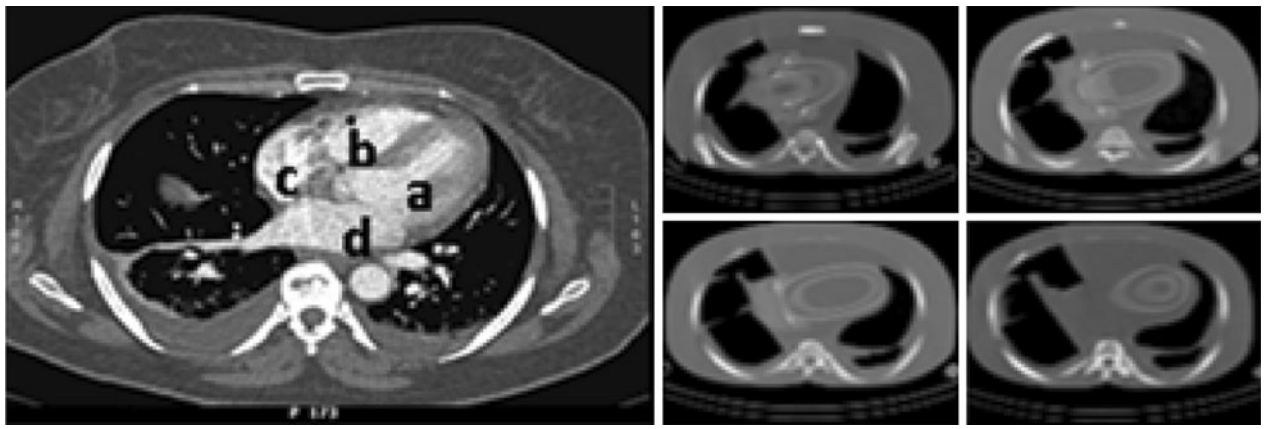

Figure 4. Transverse chest CT slices of a normal heart (*left*) obtained at NGH (*a* left ventricle, *b* right ventricle, *c* right atrium, *d* left atrium) and of the cardiac phantom at diastole (*right*) within the average male body type of the anthropomorphic phantom. The position of the cardiac phantom (left ventricle) within the anthropomorphic phantom is very close to the position of a normal heart.

in the average male body type of the anthropomorphic phantom. The position of the cardiac phantom (left ventricle) within the anthropomorphic phantom is very close to the position of a normal heart.

Image Acquisition and Reconstruction

The dynamic cardiac phantom with one or multiple defects in specific positions within the myocardial wall of the left ventricle, of specific thickness and extent, were inserted in the anthropomorphic phantom (average male, large male, large female) as described above and scanned using two different modalities: (a) the GE Millennium VG/Hawkeye (SPECT/CT) with the Entegra workstation, located at the Nicosia General Hospital (NGH) and (b) the Philips Forte/Vantage (SPECT/^{153}Gd) with the JetStream workstation, located at the Limassol General Hospital (LGH).

We performed NC, AC and GSPECT acquisitions using 22.2 MBq of ^{99m}Tc. The available scanners and processing software could apply attenuation correction on non-gated studies only.

The acquisition protocol at NGH consisted of two Low Energy High Resolution (LEHR) collimators in L-shape position. Sixty projections were acquired per scan. For the imaging, a 20% energy window was centred on the 140 keV photopeak of ^{99m}Tc. Eight gates per cycle were recorded for the gated acquisitions. The gantry performed a 90° rotation (135°-225°), thus covering 180° (dual-head). The attenuation correction was performed by acquiring low dose CT slices over the region of the heart.

The acquisition protocol at LGH consisted of 64 projections. All other acquisition parameters were the same as for the acquisition protocol at NGH.

The FBP image reconstruction algorithm was available on both workstations and it was utilized to process the NC images. The AC images were processed using the OSEM iteration algorithm on the Entegra workstation (2 iterations, 10 subsets), while the MLEM iteration algorithm was utilized on the

Table 1. Number of evaluated defects inserted in the cardiac phantom which was placed in three different body types. The acquired images for these defects were obtained at the Nicosia General Hospital (NGH) and at the Limassol General Hospital (LGH), with non-gated and gated SPECT (GNC), and attenuation corrected (AC) techniques and for two thicknesses (0.5, 1 cm) of defects

Body type	Hospital	GNC, AC	Thickness
Average male 50	NGH: 18	GNC: 8	6, 2
		AC: 10	6, 4
	LGH: 32	GNC: 16	12, 4
		AC: 16	12, 4
Large male 38	NGH: 14	GNC: 8	6, 2
		AC: 6	4, 2
	LGH: 24	GNC: 12	8, 4
		AC: 12	8, 4
Large female 54	NGH: 34	GNC: 18	16, 2
		AC: 16	14, 2
	LGH: 20	GNC: 10	6, 4
		AC: 10	6, 4

Defect position: apical (42), anterior (63), inferior (37)

JetStream workstation (30 iterations). The Butterworth filter was utilized at NGH (critical frequency: 0.4 cycles/cm, order: 10) and at LGH (critical frequency: 0.66 cycles/pixel, order: 5). Scatter correction was applied on the AC images at NGH and LGH.

From the obtained images, 142 defects were evaluated for various phantom, acquisition and reconstruction parameters as shown in Table 1.

Evaluation of Diagnosis

The physician reported a diagnosis on the defect position and severity or decided that the image quality was not adequate to perform diagnosis (uninterpretable images). Note that the physician's diagnosis was performed without having prior knowledge of the defect parameters. As the defect volume was less than a segment, the defect extent was not taken into consideration for the statistical analysis.

We then categorized the diagnoses into: (a) correct diagnosis where both defect position and severity were correctly identified, (b) over-diagnosis where the defect position was correctly identified but the defect severity was overestimated, (c) under-diagnosis where the defect position was correctly identified but the defect severity was underestimated, (d) missed defect diagnosis where the inserted defect could not be identified on the image, (e) false-defect diagnosis where a non-existent defect was identified and (f) uninterpretable diagnosis where poor image quality prevented any diagnosis to be performed.

Considering the correct, over- and under-diagnosis as the true-positive (TP) diagnosis, and the missed-defect diagnosis as the false-negative (FN) diagnosis, we calculated the diagnostic sensitivity (Sens) of the NC SPECT, AC SPECT and GSPECT studies, as: Sens = (TP)/(TP + FN). A P value of less than .05 was considered statistically significant.

RESULTS AND DISCUSSION

The diagnostic sensitivity of NC SPECT, AC SPECT and GSPECT studies for transmural and subendocardial defects (a) in three body types and (b) in the three main areas of left ventricles were investigated. The uninterpretable images were 0% from NC, 2% from AC and 6% from GSPECT studies.

First, we present in Figure 5 the short-axis slices (left column) and CT slices (right column) for the average male (upper), the large male (middle) and the large female (bottom), with no heart defects, obtained at NGH. The additional attenuation material from the large female and large male reduced the counts in the inferoseptal and anterolateral myocardial wall. This effect is more pronounced for the large female.

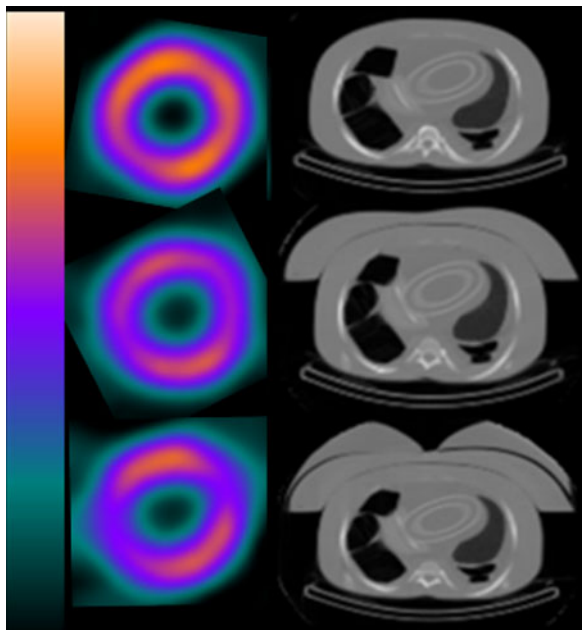

Figure 5. The short-axis slices (*left column*) and CT slices (*right column*) for the average male (*upper*), the large male (*middle*) and the large female (*bottom*), with no heart defects obtained at NGH. The additional attenuation material from the large male and large female reduced the counts in the inferoseptal and anterolateral myocardial wall. This effect is more pronounced for the large female.

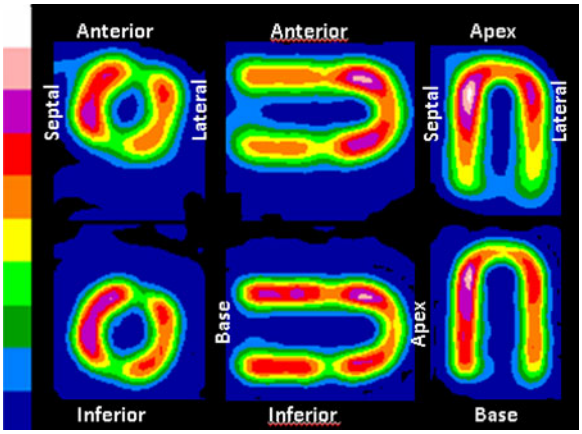

Figure 6. The short-axis (*left*), the vertical long-axis (*middle*) and the horizontal long-axis (*right*) for the non-attenuation corrected (*upper column*) and attenuation corrected (*bottom column*) images of the pumping heart placed within the average male body type of the anthropomorphic phantom, obtained at LGH. Two transmural defects, 2 × 2 cm in extent, were inserted into the heart, in the mid-anterolateral and in the mid-inferoseptal positions.

Figure 6 shows the short-axis (left), the vertical long-axis (middle) and the horizontal long-axis (right) for the NC (upper column) and AC (bottom column) images, obtained at LGH, of the pumping heart placed within the average male body type of the anthropomorphic phantom. Two transmural defects, 2 × 2 cm in extent, were inserted into the heart, in the mid-anterolateral and mid-inferoseptal positions. Further, Figure 7 presents the polar maps of the NC (left column) and AC (right column) images of the pumping heart placed within the (a) average male, (b) large male and (c) large female anthropomorphic phantom, obtained with the SPECT/CT at NGH. Two transmural defects, 2 × 2 cm in extent, were inserted into the heart, one in the apical-septal (grey arrow) and the other in the mid-anterior (white arrow) position. The additional material added to the anterior part of the anthropomorphic phantom for the large male and large female attenuated further the signal. The diagnosis was improved after applying attenuation correction techniques.

Figure 8 presents the diagnostic evaluation for identifying subendocardial defects from NC, AC and GSPECT MPI, obtained at NGH and LGH. The diagnostic sensitivity for identifying the defects in NC studies was 0.79, in AC studies was 0.82 and in GSPECT studies was 0.9. The increase in the diagnostic sensitivity between NC and AC, and between NC and GSPECT, was statistically significant ($P < .05$). The percentage of correct diagnosis was increased, while the percentage of missed-defect diagnosis was reduced when applying AC or GSPECT. Furthermore, the columns in the figure are subdivided to subendocardial

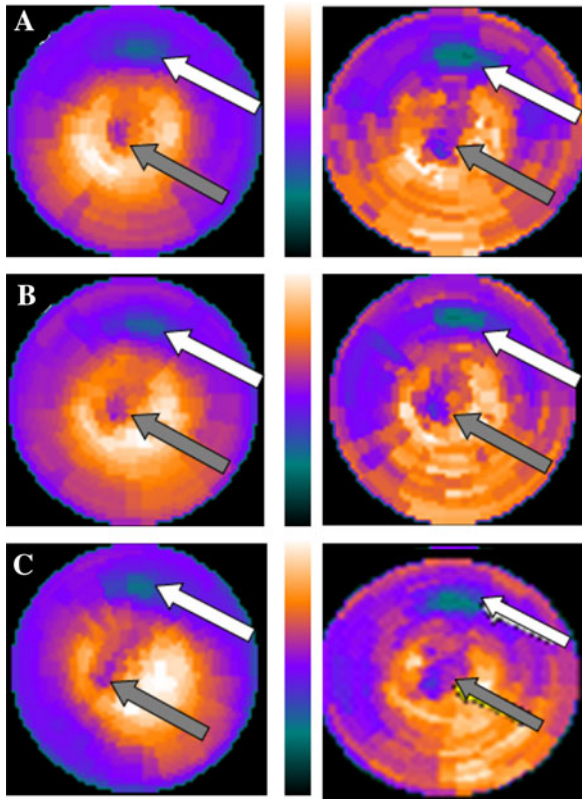

Figure 7. Non-attenuation corrected (*left column*) and attenuation corrected (*right column*) polar maps of the pumping cardiac phantom, obtained with the GE Millenium VG/Hawkeye SPECT/CT, placed within the (**A**) average male, (**B**) large male and (**C**) large female body types of the anthropomorphic phantom. Two transmural defects, 2 × 2 cm in extent, were inserted into the cardiac phantom, one in the apical-septal (*grey arrow*) and the other in the mid-anterior (*white arrow*) position. The additional material added to the anterior part of the anthropomorphic phantom for the large male and large female attenuated further the signal. The diagnosis was improved after applying attenuation correction techniques.

defects in the inferior, anterior and apical segments of the myocardial wall of the left ventricle to show the influence of NC, AC and GSPECT. Mostly, anterior defects were over-diagnosed, while inferior defects tend to be missed. This is related to the increased attenuation in the inferior wall of the LV (missed defects). The diagnostic sensitivity of NC, AC and GSPECT on subendocardial defects in the inferior, anterior and apical segments of the myocardial wall of the left ventricle is presented in Table 2. AC or GSPECT increased the diagnostic sensitivity for these defects ($P < .05$). All transmural defects were identified in all NC, AC and GSPECT MP images.

The influence of AC and GSPECT on the diagnostic sensitivity of subendocardial defects in the three body types is presented in Table 3. The AC, compared to NC,

increased the diagnostic sensitivity for identifying subendocardial defects in the average male from 0.68 to 0.83 ($P < .05$), in the large male from 0.83 to 0.88 ($P < .05$), and in the large female from 0.68 to 0.78 ($P < .05$). The GSPECT, compared to NC, increased the diagnostic sensitivity for identifying subendocardial defects in the average male from 0.68 to 0.83 ($P < .05$), in the large male from 0.83 to 1.00 ($P < .05$) and in the large female from 0.68 to 0.88 ($P < .05$). All body types benefited from AC or GSPECT.

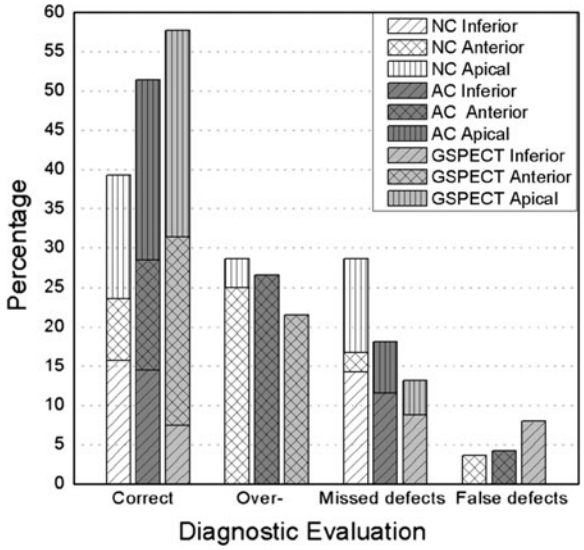

Figure 8. Diagnostic evaluation of subendocardial defects from non-attenuation corrected (NC), attenuation corrected (AC) and GSPECT MPI, obtained at NGH and LGH. The increase in the diagnostic sensitivity between NC and AC, and between NC and GSPECT, for inferior, anterior and apical defects was statistically significant ($P < .05$).

CONCLUSIONS

In this study, we present our first results on the diagnostic sensitivity of MPI using the constructed pumping cardiac phantom with inserted variable defects. A diagnosis blinded to prior-known conditions was performed to evaluate the CAD. NC, AC and GSPECT techniques were investigated for various phantom configurations.

Attenuation correction or gating techniques increased the percentage of correct diagnosis and reduced the percentage of missed-defect diagnosis. AC or GSPECT increased the diagnostic sensitivity compared to NC. In particular, the diagnostic sensitivity was improved for subendocardial defects in the inferior, anterior and apical segments of the myocardial wall of the left ventricle for all three body types, while transmural defects could be identified without any attenuation correction or gating.

This methodology allows investigating and evaluating the sensitivity of MPI techniques without exposing patient to radiation in order to determine the most

Table 2. Diagnostic sensitivity (Sens) and statistical *P* value of non-attenuation corrected (NC), attenuation corrected (AC) and GSPECT MPI, obtained at NGH and LGH, for subendocardial defects in the anterior, inferior and apical segments of the myocardial wall of the left ventricle

	Sens			*P*	
Subendocardial defects	**NC**	**AC**	**GSPECT**	**NC-AC**	**NC-GSPECT**
Anterior	0.91	1.00	1.00	.01	.01
Inferior	0.56	0.85	0.88	.02	.02
Apical	0.58	0.73	0.87	.02	.01

Table 3. Diagnostic sensitivity (Sens) and statistical *P* value of non-attenuation corrected (NC), attenuation corrected (AC) and GSPECT MPI, obtained at NGH and LGH, for subendocardial defects in the average male, large male and large female

	Sens			*P*	
Body type	**NC**	**AC**	**GSPECT**	**NC-AC**	**NC-GSPECT**
Average male	0.68	0.83	0.83	.001	.001
Large male	0.83	0.88	1.00	.02	.02
Large female	0.68	0.78	0.88	.001	.03

appropriate and cost-effective technique for CAD diagnosis.

In this study, the sensitivity was only measured. The specificity is also important when evaluating different means of acquiring and/or processing AC and GSPECT data. A change in methodology, such as using a different reconstruction algorithm, may improve sensitivity while at the same time reducing specificity. Next studies will include measurements of sensitivity as well as of specificity.

In the future, we will investigate more phantom and processing parameters for further MPI optimization. The improved image quality and the interpretive certainty will lead to more definite conclusions of the MPI studies for the early detection of CAD and its effective treatment.

Acknowledgments

We gratefully acknowledge all staff from the Nuclear Medicine Department of the Limassol and Nicosia General Hospitals (Neofytos Fasouliotis, Antri Panayi, Christoforos Panagidis, Andreas Mormoris. Chariklia Christodoulou, Lambros Lambrou, Charoula Charalambous, Chloe Ioannou, Katerina Hadjitoffi, Despina Demetriou) for helping in obtaining these MPIs.

References

1. European Heart Network, European Cardiovascular Disease Stastistics, 3rd edn (2008). http://www.epha.org/a/2920. Accessed 16 Jan 2012.
2. American Heart Association. Heart disease and stroke 2012 statistical update. Circulation 2012; 125: e2-e220. http://circ.ahajournals.org/content/125/1/e2.full. Accessed 16 Jan 2012.
3. Baghdasarian SB, Heller GV. The role of myocardial perfusion imaging in the diagnosis of patients with coronary artery disease: Developments over the past year. Curr Opin Cardiol 2005;20:369-74.
4. Seo Y, Mari C, Hasegawa BH. Technological development and advances in single-photon emission computed tomography/computed tomography. Semin Nucl Med 2008;38:177-98.
5. Pazhenkottil AP, Ghadri JR, Nkoulou RN, Wolfrum M, Buechel RR, Küest SM, et al. Improved outcome prediction by SPECT myocardial perfusion imaging after CT attenuation correction. J Nucl Med 2011;52:196-200.
6. Heller GV, Bateman TM, Johnson LL, Cullom SJ, Case JA, Galt JR, et al. Clinical value of attenuation correction in stress-only Tc-99m sestamibi SPECT imaging. J Nucl Cardiol 2004;11:273-81.
7. Huang R, Li F, Zhao Z, Liu B, Ou X, Tian R, et al. Hybrid SPECT/CT for attenuation correction of stress myocardial perfusion imaging. Clin Nucl Med 2011;36:344-9.
8. Wolak A, Slomka PJ, Fish MB, Lorenzo S, Berman DS, Germano G. Quantitative diagnostic performance of myocardial perfusion SPECT with attenuation correction in women. J Nucl Med 2008;49:915-22.
9. Cerqueira MD, Weissman NJ, Dilsizian V, Jacobs AK, Kaul S, Laskey WK, et al. Standardized myocardial segmentation and nomenclature for tomographic imaging of the heart: A statement for healthcare professionals from the cardiac imaging committee of the council on clinical cardiology of the American Heart Association. Circulation 2002;105:539-42.
10. El-Ali HH, Palmer J, Carlsson M, Edenbrandt L, Ljungberg M. Interdependence between measures of extent and severity of myocardial perfusion defects provided by automatic quantification programs. Nucl Med Commun 2005;26:1125-30.
11. Chrysanthou-Baustert I, Parpottas Y, Demetriadou O, Christofides S, Yiannakkaras Ch, Kaolis D et al. Monte Carlo simulations to assess differentiation between defects in cardiac SPECT. J Phys Conf Ser 2011;317:012018.
12. Radiology Support Devices, ALDERSON phantoms: Anthropomorphic phantoms for Nuclear Medicine. http://www.rsdphantoms.com/nm_heart.htm. Accessed 10 Mar 2010.